Catalysis Science and Technology 8.15 (2018): 3926-3935

DOI: https://doi.org/10.1039/c8cy00461g

Journal Name

ARTICLE

Chloroform conversion into ethane and propane by catalytic hydrodechlorination with Pd supported on activated carbons from lignin

Received 00th January 20xx,
Accepted 00th January 20xx

DOI: 10.1039/x0xx00000x

www.rsc.org/

C. Fernandez-Ruiz[a], J. Bedia*[a], P. Bonal[a], J.J. Rodriguez[a], L.M. Gómez-Sainero[a]

Conversion of chloroform (TCM) by gas-phase catalytic hydrodechlorination (HDC) has been addressed to maximize the selectivity to ethane and propane. Several own-made Pd (1 wt.%) catalysts have been tested. The catalysts were prepared by incipient wetness impregnation of five different activated carbons. These carbons were obtained by chemical activation of lignin with different activating agents, namely, H_3PO_4, $ZnCl_2$, $FeCl_3$, NaOH and KOH. The catalysts were fully characterized by N_2 adsorption-desorption at -196 ºC and CO_2 adsorption at 0 ºC, TPR, NH_3-TPD, XRD, XPS and TEM. The activating agent conferred important differences on the characteristics of activated carbon supports, and hence to the resulting catalysts, in terms of porous texture, surface acidity, Pd oxidation state and Pd particle size distribution. NaOH and KOH activation led to carbons with the highest surface areas (2158 and 2991 $m^2 \cdot g^{-1}$, respectively) and low Pd^0/Pd^{n+} ratio, while $ZnCl_2$- and H_3PO_4-activated carbons yielded the highest surface acidity and mean Pd particle sizes. The analysis of the TOF values revealed that HDC of TCM on these catalysts is a structure-sensitive reaction, increasing TOF values with Pd particle size. The best results, in terms of selectivity to ethane and propane, were obtained with the catalysts supported on KOH and NaOH activated carbons. The former allowed 80% selectivity to those target compounds at almost complete dechlorination (> 99%) at 300 ºC. The KOH-based catalysts showed fairly good stability at 200 ºC reaction temperature.

1. Introduction

The use, structure and removal treatments of chloromethanes have been widely studied due to their harmful properties related with air and water contamination. They are involved in stratospheric ozone depletion, smog formation and global warming effect.[1] Furthermore, these vapours are harmful for human health resulting in breathing problems, burning and redness on contact with skin, cancer diseases, etc.[2] Among them, chloroform (TCM) and dichloromethane (DCM) are commonly used in several industries as automotive repairing products, on the manufacture of photographic film, refrigerants, industrial solvents and as chemical intermediates.[3] As a consequence, governments and international regulations have limited their emissions in the last years, leading to the need of developing new technologies for the treatment of chloromethanes in residual streams. Several techniques are available for this purpose but recycling to valuable products becomes more interesting.

There is a huge world demand of light paraffins and olefins, because these compounds constitute basic raw materials in the chemical industry to produce solvents, polymers and cosmetics, among other. They are mainly produced from fossils raw materials, not renewable, by different industrial processes, which present serious drawbacks such as, high energy demand, low selectivity and dependency of the unstable oil prices. Ethane and propane are components of natural gas (separated by cryogenic liquefaction) and they constitute very important petrochemical feedstocks. These compounds are used as raw materials for the synthesis of the irreplaceable olefins by oxidative dehydrogenation. These factors underline the importance of the investigation of alternative processes to produce these compounds.

Hydrodechlorination is a very suitable technology for the treatment of chloromethanes,[4,5] being its main advantage that it operates under moderate conditions of temperature and pressure. This technique has also been used for the hydrodechlorination of chlorophenols and their derivates in water with the aim of converting these pollutants into species of much lower toxicity.[6-9] In gas phase, TCM and DCM are mainly converted to methane, while lower selectivities to other products and by-products that could have industrial interest are obtained. The valorisation of chloromethanes to light paraffins (other than methane) and/or olefins (C2-C3) would be of more interest. Moreover, a lower amount of H_2 would be needed, which results in economic benefit for the process. The studies reported in the bibliography about chloromethanes (other than carbon tetrachloride) treatment are mainly focused in the removal of the pollutant with very few works concerning to the production of C2-C3 hydrocarbons by this methodology.[10-12]

Gas-phase catalytic hydrodechlorination (HDC) has been mainly studied using catalysts based on metallic active phases supported on a porous support.[13-16] Many active metallic phases have been studied to compare their activity on the catalytic hydrodechlorination.[17] Our research group has reported recently a study focused in the valorisation of chloromethanes to C2-C3 hydrocarbons.[18] It includes simulation and experimental

[a] Sección de Ingeniería Química, Facultad de Ciencias, Universidad Autónoma de Madrid, Cantoblanco, 28049 Madrid, Spain. E-mail: jorge.bedia@uam.es.
Electronic Supplementary Information (ESI) available: [details of any supplementary information available should be included here]. See DOI: 10.1039/x0xx00000x

analysis, comparing the catalytic HDC using Ru, Rh, Pt and Pd supported on activated carbon. It was concluded that the active phase with the highest selectivity to hydrocarbons with more than one atom of carbon (that is to say, other than methane) was Pd. Pd based catalysts are being commonly studied for the catalytic HDC on many different types of supports, such as, Al_2O_3, SAPO-34, CeO_2, SiO_2, activated carbons and many others.[4,5,15,19]

Lignin is a by-product of the pulp and papermaking industry, which is mainly used for its fuel value. It has been also evaluated as raw material for the synthesis of carbon materials, such as activated carbons[20,21] or carbon-based catalysts or catalyst-supports.[22-24] In previous studies,[13,18] the results suggested that selectivity to ethane and propane was influenced by metal oxidation state and particle size. These and other characteristics of the catalysts such as, porosity or acidity can be in part conferred by the support.[25,26] The objective of this work is to evaluate the performance of Pd supported on chemically activated carbons from lignin for the valorisation of chloroform by HDC to produce high valued hydrocarbons with more than one carbon atom. Five Pd based catalysts were synthesized by deposition of the active phase on activated carbons obtained by chemical activation of lignin with $FeCl_3$, NaOH, KOH, $ZnCl_2$ and H_3PO_4, to confer different physico-chemical properties to the catalysts.

2. Experimental

2.1. Materials and chemicals

Lignin (C: 61.6%; H: 6.0%; N: 1.1%; S :0.2%; ash content = 2.0 wt.%) was purchased from Granit S.A. (Switzerland) and used as received. $ZnCl_2$ (>99%), KOH pellets (>85%), H_3PO_4 (85%), $PdCl_2$ (99%) and HCl (37%) were supplied by Panreac, while $FeCl_3$ anhydrous (>98%) was obtained from Riedel-de Haën and NaOH pellets (>95%) from Sharlau. The gas chloroform (1.5% mol in N_2), H_2 and N_2 (both 99.999% purity) were provided by Praxair.

2.2. Synthesis of the catalysts

Five activated carbons were synthesized as supports by chemical activation of lignin using $FeCl_3$, $ZnCl_2$, H_3PO_4, KOH and NaOH as activating agents. In the case of activation with $FeCl_3$, $ZnCl_2$ or H_3PO_4, lignin samples were physically mixed with the corresponding activating agent, using an activating agent: precursor mass ratio, R, equal to 3:1, and dried for 24 h at 60 ºC. The impregnated samples were heat-treated in a tubular furnace under continuous N_2 flow (250 $Ncm^3 \cdot min^{-1}$) at activation temperatures of 500 ºC in the case of $ZnCl_2$ and H_3PO_4 and 800 ºC with $FeCl_3$. The activation temperature was reached at 10 ºC·min^{-1} heating rate and maintained for 2 h. In the case of NaOH and KOH-activations, lignin was previously carbonized at 500 ºC at the same aforementioned conditions and then activated at 800 ºC using an activating agent:lignin mass ratio of 4:1. After cooling down to room temperature under the same N_2 atmosphere, the samples were washed with a 0.1M HCl aqueous solution at 70 ºC under continuous stirring for 3h using 200 cm^3 of HCl aqueous solution per gram of sample, rinsed with distilled water until neutral pH of the eluate and finally dried for 24h at 60ºC. This acid washing procedure removes the activating agent releasing the blocked porous structure. The activated carbons synthesized were denoted by an acronym related to the activation agent used in its synthesis, followed by the mass ratio (R) and the activation temperature, namely, Fe3-800, Zn3-500, P3-500, Na4-800 and K4-800.

Pd was deposited on the activated carbons by incipient wetness impregnation, with a $PdCl_2$ 1M HCl aqueous solution, to obtain a nominal 1.0 wt.% of Pd. After impregnation, the samples were dried overnight in an oven at 70 ºC. The catalysts were denoted with the name of the activated carbon used as support followed by Pd, namely, Fe3-800-Pd, Zn3-500-Pd, P3-500-Pd, Na4-800-Pd and K4-800-Pd.

2.3. Characterization

Prior to the characterization, all the catalysts were reduced under H_2 flow (50 $Ncm^3 \cdot min^{-1}$) at 250 ºC for 2 h in order to analyse them in the same conditions used for the reaction test (except for TPR analyses which were performed using the non-reduced catalysts). The porous structure was evaluated by N_2 adsorption-desorption at -196ºC and CO_2 adsorption at 0ºC (the latter for the characterization of the narrow microporosity, 0.7 < size < 2.0 nm) on a Tristar II 3020 apparatus (Micromeritics). The samples were previously outgassed for at least 12 h at 150 ºC until residual pressure with a VacPrep 061 apparatus (Micromeritics). BET equation was used to calculate the specific surface area (A_{BET}).[27] The t-method was applied to obtain the micropore volume (V_{micro}) and the external surface area (A_{ext}).[28] The total pore volume was estimated from the amount of N_2 adsorbed at P/Po ≈ 0.99 converted in liquid volume (V_{pore}). The narrow micropore volume (V_{DA}) and area (A_{DA}) were obtained applying the Dubinin-Astakhov method[29] to the CO_2 isotherm.

The crystalline structure of the catalysts was analysed by X-ray diffraction (XRD) (X'Pert PRO Panalytical Diffractometer). The powdered samples were scanned using CuKα monochromatic radiation (λ = 0.15406 nm) and a Ge mono filter. A scanning range of 2θ = 10-100º and a scan step size of 0.020º with 5 s collection time were used.

The total acidity and acid strength distribution of the catalysts have been determined by temperature programmed desorption of ammonia (NH_3-TPD) using an AutoChem II 2920 unit. The NH_3-TPD was performed using 10 mg of catalysts saturated with 25 $Ncm^3 \cdot min^{-1}$ of NH_3/He 5% at 100 ºC. After saturation, the NH_3 weakly adsorbed was desorbed in a He flow (25 $Ncm^3 \cdot min^{-1}$), at the adsorption temperature, until no NH_3 was detected in the outlet gas. The NH_3-TPD was performed by raising the temperature up to 940 ºC at a heating rate of 10 ºC·min^{-1}. The NH_3 desorbed was monitored with a Thermal Conductivity Detector (TDC) recording one measurement per second.

The reduction at programmed temperature (TPR) analysis were performed in a Chemisorb 2720 apparatus (Micromeritics) equipped with a TCD. The samples were previously purged with He and TPR analysis was carried out using 10%H_2/Ar (50 $Ncm^3 \cdot min^{-1}$) from room temperature up to 625 ºC with a heating rate of 10 ºC·min^{-1}.

The palladium metal content was determined using inductively coupled plasma-mass spectroscopy (ICP-MS Elan 6000, Perkin-Elmer Sciex). The samples were previously digested in a strongly acidic mixture (HNO_3:3HCl) and treated in a microwave oven (Milestone ETHOS PLUS).

The external surface composition of the reduced catalysts was analysed by X-ray photoelectron spectroscopy (XPS) with a Thermo Scientific apparatus with Al Kα radiation (1486.7 eV).

General spectra were recorded for the samples by scanning binding energy (BE) from 0 to 1200 eV. Corrections for changes in BE caused by sample charging were corrected by taking the C1s peak (284.6 eV) as an internal standard.

The Pd particle size distribution and morphologies were analysed by Transmission Electronic Microscopy (TEM). The TEM images were obtained using a Tecnai G220 microscope from FEI COMPANY at an accelerating voltage of 200 kV. Particle size distributions were obtained by measurement of at least 100 particles.

2.4. Gas-phase HDC tests

The HDC experiments were performed in a continuous flow reaction system (Micro-Activity by PID) described elsewhere,[13] using a quartz fixed bed micro-reactor (4 mm internal diameter). Prior to reaction, the catalysts were reduced "in situ" under a H_2 flow (50 $Ncm^3 \cdot min^{-1}$) at 250 ºC for 2 h. The operating conditions were atmospheric pressure, a total flow rate of 100 $Ncm^3\ min^{-1}$, an inlet chloroform (TCM) concentration of 1000 ppmv with a H_2/TCM molar ratio of 100:1. The catalyst weight was 0.213 g resulting in a space time of 0.8 $kgcat \cdot h \cdot mol^{-1}$ TCM. Reaction temperature was increased from 75 to 200 ºC at 10 $ºC \cdot min^{-1}$ heating rate. The reactor outlet was coupled to a gas chromatograph (Varian 450-GC), equipped with a FID detector and a capillary column (Varian, CP-SilicaPLOT, 60 m). The carbon mass balances were checked and never showed deviations higher than 5%.

The performance of the catalysts was evaluated in terms of TCM conversion (X), turnover frequency (TOF) and selectivity to the different reaction products (S_i). The values of turnover frequency were calculated as the moles of reactant converted per mole of surface-exposed Pd atoms. The dispersion values were calculated assuming spherical metallic particles using the equation:[30]

$$D(\%) = \frac{6 \cdot 10^5 \cdot M_w}{\rho_M \cdot \sigma_M \cdot N_A \cdot d}$$

where M_w corresponds to the atomic mass of Pd (106.42 $g \cdot mol^{-1}$), ρ_M is the density of the metal (12.02 $g \cdot cm^{-3}$ for Pd), σ_M represents the effective surface area of a Pd atoms ($7.87 \cdot 10^{-20}$ $m^2 \cdot atom^{-1}$), N_A is the Avogadro's number and d is the mean metal particle size (obtained from TEM) in nm. The amount of exposed metal atoms was calculated from the nominal content of Pd in µmol per gram of catalysts multiplied by the corresponding dispersion values.

3. Results and discussion

3.1 Characterization of the catalysts

Figures 1 and ES1 (Electronic Supplementary Information) depict the N_2 adsorption-desorption isotherms at -196 ºC of the catalysts and activated carbons synthesized, respectively. The deposition of Pd on the surface of the activated carbons did not modify significantly the N_2 adsorption-desorption isotherms. The isotherms of K4-800-Pd, Na4-800-Pd and Fe3-800-Pd are of type I according to the IUPAC classification, characteristics of predominantly microporous materials. The wider knee at low relative pressures (P/Po<0.4) of KOH and NaOH based catalysts suggests the presence of a wide microporous size distribution in these samples. In contrast, Zn3-500-Pd and P3-500-Pd catalysts exhibited type IV isotherms associated to mesoporous materials with a significant contribution of microporosity. These isotherms show H4 hysteresis cycles, commonly seen on activated carbons. Tables 1 and ES1 summarize the parameters characteristic of the porous structure of the catalysts and activated carbons, respectively, obtained from the N_2 adsorption-desorption and CO_2 adsorption isotherms (CO_2 adsorption was measured only for the catalysts). The comparison between both tables reveals a very slight reduction of porosity once Pd active phase is deposited, probably because of the partial blockage of some pores by the deposited Pd atoms, as previously observed for other metal supported on activated carbon catalysts.[22] The low porosity contraction is due to the relatively low amount of Pd deposited (1wt.%). All the catalysts show high specific surface areas, from the 500 $m^2 \cdot g^{-1}$ of P3-500-Pd up to the very noteworthy more than 2100 and almost 3000 $m^2 \cdot g^{-1}$ of Na4-800-Pd and K4-800-Pd, respectively. It is well-known that chemical activation with NaOH or KOH results in activated carbons with very well developed porous structures, and in some cases total surfaces areas higher than 3000 $m^2 \cdot g^{-1}$ like the obtained in this work (Table ES1).[31,32] The rest of surface areas are in the range of those previously reported in the literature for carbons prepared from chemical activation of lignin.[33-36] Therefore, the chemical activation of lignin and subsequent Pd deposition allows to obtain catalysts with well-developed and tuneable porosity. It is also noteworthy the high narrow micropore surface area (A_{DA}) and volume (V_{DA}) obtained for all the catalysts. The ratio A_{DA}/A_{BET} gives an idea of the pore size distribution. Values of this ratio close to 1 are related with relatively homogeneous micropore size distribution, ratios higher than 1 are characteristic of a predominantly narrow microporosity and ratios lower than 1 of materials with relatively wide microporosity. Fe3-800-Pd catalysts shows the narrowest micropore size distribution, while Zn3-500-Pd has the widest. On the other hand, Na4-800-Pd and specially K4-800-Pd exhibited the most homogeneous micropore size distributions with A_{DA}/A_{BET} ratios close to 1.

Figure 2 depicts the TPR profiles of the fresh catalysts. All of them show similar profiles with high intensity peaks (in some cases with a shoulder) at lower temperatures (< 300 ºC) and broad bands at higher temperatures (> 400 ºC). The maximums of the low temperature peaks are located between 165 and 250 ºC and are indicative of the H_2 consumption during the reduction of oxy- and/or hydroxy-Pd species.[37] The peak displacement towards higher temperatures could be related to a stronger interaction of the Pd particles with the support.[38] The reducibility of the catalysts follows the order P3-500-Pd > Zn3-500-Pd ≈ Fe3-500-Pd > K4-800-Pd > Na4-800-Pd. The shoulders

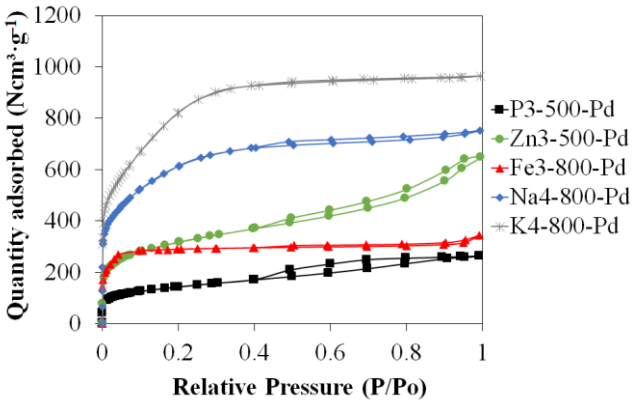

Fig. 1 N_2 adsorption-desorption isotherms of the catalysts at -196 ºC

Table 1 Characterization of the porous texture of the catalysts.

Catalyst	N_2 isotherms			CO_2 isotherms			
	A_{BET} ($m^2 \cdot g^{-1}$)	V_{micro} ($cm^3 \cdot g^{-1}$)	A_{ext} ($m^2 \cdot g^{-1}$)	V_{pore} ($cm^3 \cdot g^{-1}$)	V_{DA} ($cm^3 \cdot g^{-1}$)	A_{DA} ($m^2 \cdot g^{-1}$)	A_{DA}/A_{BET}
Fe3-800-Pd	852	0.43	41	0.53	0.17	953	1.12
Zn3-500-Pd	1103	0.23	594	1.00	0.12	848	0.77
P3-500-Pd	501	0.08	315	0.41	0.07	426	0.85
Na4-800-Pd	2158	0.95	186	1.17	0.15	1936	0.90
K4-800-Pd	2991	1.34	157	1.49	0.18	2845	0.95

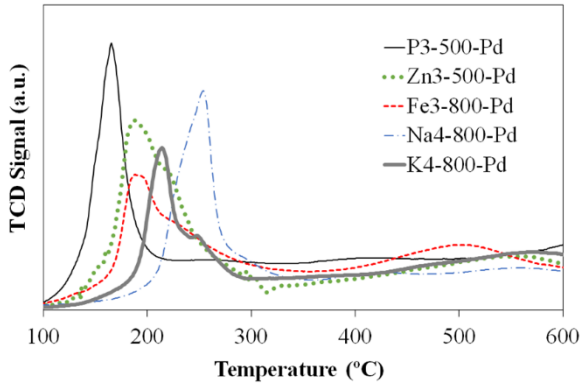

Fig. 2 TPR profiles of the different catalysts in 10% H_2/Ar (50 $cm^3 \cdot min^{-1}$).

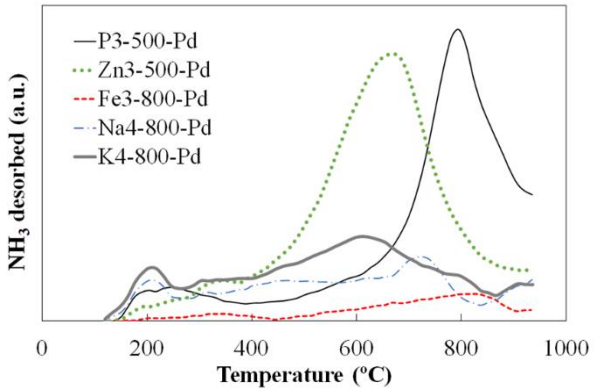

Fig. 3 NH_3-TPD curves of the catalysts.

observed in the low temperature peaks of some of the catalysts could be explained by the reduction of Pd species located on the pores with more restrictive access. The presence of these shoulders may be related to different interactions of palladium with the support. These interactions can be more pronounced in the smallest pores because of the proximity of the walls, thus giving rise to the observed shoulders at higher reduction temperature in the TPR profiles. Examples of geometric interaction of supported Pd particles leading to several peaks at different reduction temperature can be found in the literature.[39-40] Finally, the broad bands observed at reduction temperatures higher than 400 ºC could be due to the interaction of H_2 with the surface of carbons, possibly favoured by spillover phenomena promoted by surface oxygen groups. Hydrogen that spilt over could adsorb on the carbon surface promoting the reduction of surface oxygen groups and hydrogasification reactions.[41,42] To confirm this, we have performed TPR analyses to the bare activated carbons prior to palladium deposition. As can be seen in the figure below (Figure ES2), the reduction peaks observed for the catalysts below 300 ºC (Figure 2) are not present in the case of activated carbons. This result discards a significant effect of the surface O-containing functionalities on the H_2 consumption, specially at temperatures below 300 ºC

The surface acidity was studied by ammonia temperature programmed desorption (NH_3-TPD). Figure 3 represents the NH_3-TPD profiles of the catalysts, where the NH_3-desorption temperature and the intensity of the peaks are related to the strength and amount of the acid sites, respectively. $FeCl_3$ derived catalyst showed the lower amount of surface acid sites confirming its very low acidity. In contrast, Zn3-500-Pd and P3-500-Pd exhibited much higher acidity than the rest of the catalysts. Furthermore, it is noteworthy that P3-500-Pd showed high strength acid sites desorbing at temperatures higher than 600 ºC. The high acidity of phosphoric acid-derived activated carbons is in agreement with previously reported results suggesting that it is related to the remaining phosphorus from the activating agent retained onto the carbon surface, probably associated to OH groups in phosphates.[43,44] The other catalysts, obtained by activation with alkali hydroxides, Na4-800-Pd and K4-800-Pd, exhibited low acidity. The presence of a significant amount of acid sites on these catalysts, despite their activation with NaOH or KOH, could be related to the acid washing performed after the activation procedure (0.1M HCl aqueous solution, 70 ºC, 3h) carried out to extract the rests of the activating agents from the porous structure. We could conclude that the surface acidity of the synthesized catalysts follows the order P3-500-Pd ≈ Zn3-500-Pd >> K4-800-Pd > Na4-800-Pd > Fe3-800-Pd. The surface acidity seems to be highly dependent on the activating agent used in the synthesis of the porous support.

The palladium metal contents, determined by ICP, are summarized in Table ES2. The bulk contents are in all the cases very similar to the nominal ones confirming the success of the deposition step. The Pd distribution through the particles of the catalysts and its oxidation state were analysed by XPS. Table 2 summarizes the Pd mass and atomic surface concentrations. As can be seen, both atomic and mass Pd external concentration follow quite similar trends. Taking into account that the theoretical bulk load of Pd was set at 1 wt.%, it could be seen that Fe3-800-Pd and P3-500-Pd catalysts show homogeneous Pd distribution with similar bulk and external Pd contents. In contrast, K4-800-Pd shows a higher proportion of Pd located on the external surface (egg-shell distribution) while Na4-800-Pd and Zn3-500-Pd exhibited a higher proportion of Pd in the inner of the catalyst particles (egg-yolk distribution). Pd3d XPS region presents a doublet corresponding to Pd $3d_{5/2}$ and Pd $3d_{3/2}$ with a quantified separation of 5.3 eV, due to spin orbital splitting.[45] The Pd $3d_{5/2}$ peak centred at approximately 335.5 eV can be assigned to Pd^0 (metallic Pd), while the one lying near 338.0 eV corresponds to Pd^{n+} (electrodeficient palladium).[39,46] Figure 4

represents the deconvoluted Pd 3d spectra of all the catalysts and Table 2 shows the Pd^0/Pd^{n+} ratios obtained from these deconvolutions. If we analyse the position of the Pd $3d_{5/2}$ peak, it could be seen a clear displacement of the XPS profiles to higher binding energies following the order Fe3-800-Pd > P3-500-Pd ≈ Zn3-500-Pd > Na4-800-Pd ≈ K4-800-Pd (from lower to higher binding energies). This order is the same of the Pd^0/Pd^{n+} ratio obtained from the deconvoluted spectra and depicted in Table 2 since the signal of Pd^0 is located at lower binding energies than the Pd^{n+}. Fe3-800-Pd catalysts show the highest Pd^0/Pd^{n+} ratio while Na4-800-Pd and K4-800-Pd exhibited the lowest ones with more contribution of electrodeficient Pd. This behaviour, in general trend, agrees with the results of the H_2-TPR profiles (Figure 2), which showed that Na4-800-Pd and K4-800-Pd catalysts needed higher temperatures to reduce completely the Pd species.

XRD patterns (Figure ES3) showed no peaks due to Pd reflections probably as a consequence of the low content and/or small particle size, suggesting a high dispersion of the palladium particles. P3-500-Pd, Zn3-500-Pd and Fe3-800-Pd XRD patterns show wide broad bands located at around 26 and 44º (corresponding to (002) and (101) set of planes of graphite, respectively). Activated carbons are formed by turbostratic carbon with stacked graphene layers regularly spaced as in graphite but with a much lower degree of stacking order.[47] In the case of these catalysts, these bands are not very intense and/or well defined, which is indicative of the low structural order of these catalysts.[48] In the case of Na4-800-Pd and K4-800-Pd, these carbon-based catalysts show no bands at all, probably due to the high structural disordered suggested by the very high porosity development of these materials. The Pd particle size distributions were analysed using transmission electronic microscopy. Figure 5 depicts representative TEM images of the different catalysts. It could be visible to the naked eye that very significant differences exist between the sizes of the Pd particles of the different catalysts. Particle size distributions (Figure ES4) and the medium particle sizes (Table 2) indicate that all the Pd particles are nanometric in size in the range of around 1.0 up to 35.0 nm with monodisperse particle size distributions for all the catalysts. The analysis of the mean particle sizes allows to recognize catalysts with low Pd particle sizes (below 5 nm), namely, Fe3-800-Pd, Na4-800-Pd and K4-800-Pd and those with higher particle sizes (> 13 nm), Zn3-500-Pd and P3-500-Pd. These significant differences can be associated to the different surface acidity of the carbon supports, with which a clear relationship seems to exist. However, a correlation with the

Table 2 Pd external mass and atomic contents and Pd^0/Pd^{n+} obtained from XPS, Pd mean particle size from TEM and dispersion.

Catalyst	XPS			TEM	
	Pd external content		Pd^0/Pd^{n+}	Pd mean particle size (nm)	Dispersion (%)
	mass (%)	atomic (%)			
Fe3-800-Pd	0.95	0.11	1.82	2.0	56.3
Zn3-500-Pd	0.60	0.07	0.65	15.3	7.3
P3-500-Pd	1.10	0.14	0.60	13.5	8.3
Na4-800-Pd	0.58	0.07	0.26	2.7	41.2
K4-800-Pd	1.25	0.16	0.21	4.7	23.9

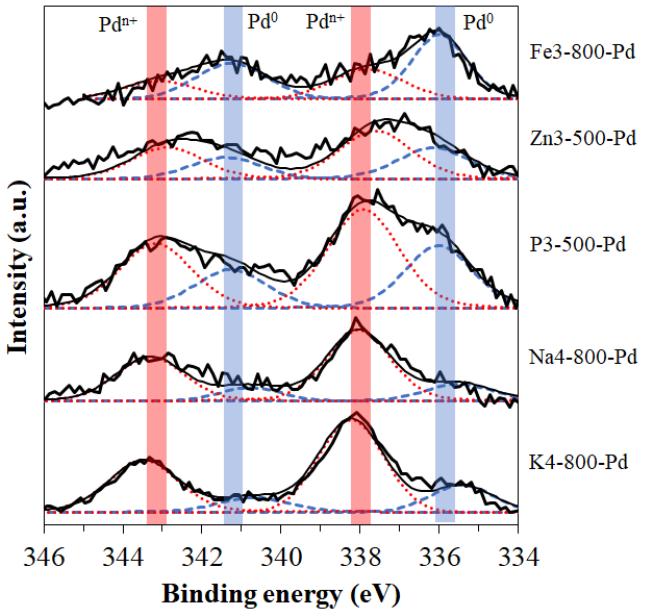

Fig. 4 Deconvoluted Pd3d spectra.

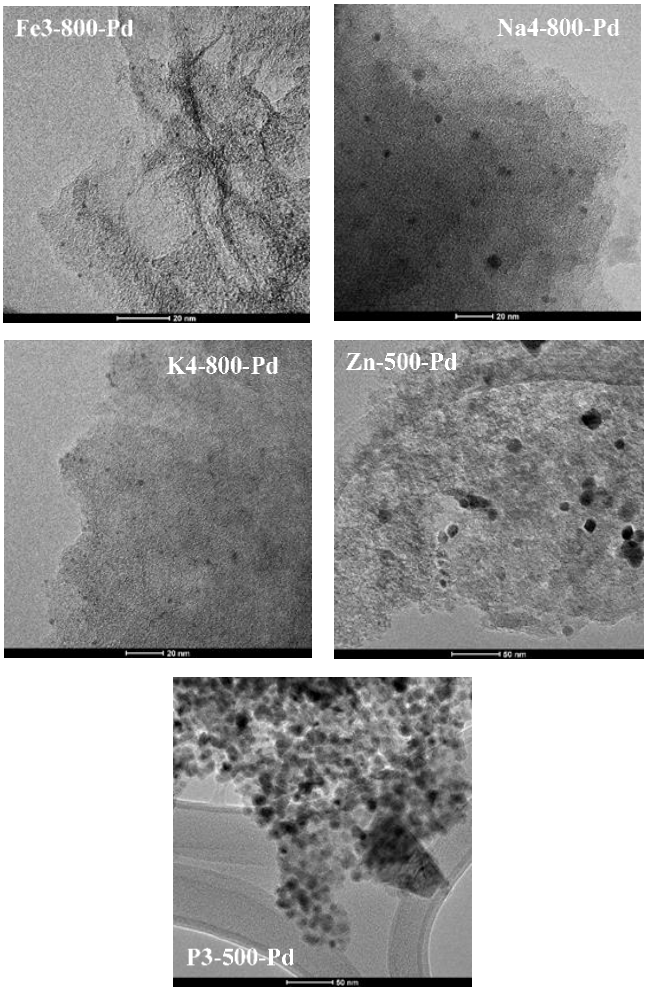

Fig. 5 Representative TEM images of the catalysts.

different pore size distribution is also found. The catalysts with the highest surface acidity, P3-500-Pd and Zn3-500-Pd, exhibited the highest mean particle sizes (13.5 and 15.3 nm, respectively), but they also show a higher contribution of mesoporosity. In contrast, Fe3-800-Pd showed the lowest surface acidity, the highest narrow micropore surface area and the lowest mean particle size (2.0 nm). It is usually accepted that dispersion is favoured by surface acidity, typically in form of oxygen surface functionalities. In our case however, the carbons with highest surface acidity showed the lowest dispersion. This behaviour has been previously observed for activated carbons treated with HCl and HNO_3, which showed a decrease of metal dispersion after these acid treatments.[42] The authors ascribed this behaviour to different possible causes such as the decrease of surface area and pore volume, enhancement of support degasification under the reductive treatment or hindering of anchorage of the Pd precursor. Further studies are necessary to clarify the contribution of these properties to the formation of metal particles.

3.2. HDC tests

Figure 6 represents the TCM conversion versus reaction temperature using all the catalysts synthesized. Conversion increases with reaction temperature. All the catalysts achieved a total TCM conversion in the temperature range analysed, and even K4-800-Pd reached a complete conversion of the chloromethane at a temperature as low as 125 ºC. The different conversion values obtained with the different catalysts appear to be a consequence of the differences in the Pd particles sizes. To shed light on the influence of the Pd particle size on the activity of the catalysts, Figure 7 represents the values of the turnover frequencies (TOFs) at 100 ºC as a function of the mean particle size. The TCM HDC on these catalysts seems to be a structure sensitive reaction, showing an increasing activity with increasing Pd particle size. This behaviour is in agreement with the previously reported by Ramos et al.[42] for the same reaction using also Pd supported on activated carbon catalysts. They reported a clear increase of the TOF values with decreasing dispersion. Table 3 summarizes the TOF values at different temperatures for the HDC of TCM on the different catalysts. TOF values in the range of around 12 to 240 h^{-1} were obtained in the temperature range analysed. Ramos et al.[42] reported very high TOF values of approximately 10080 h^{-1} over a carbon supported Pd (9 wt.%) catalyst at 100 ºC with a space velocity of 16 h^{-1} for the HDC of TCM. More similar results to those obtained in our work were shown by Martín-Martínez et al.[18] for the same reaction with TOFs between 50 and 430 h^{-1} at 150 ºC using Rh, Ru, Pd and Pt in activated carbon-supported catalysts. In the HDC of other chloromethanes, Bonarowska et al.[49] reported TOF values in the range 25-1650 h^{-1} for the HDC of tetrachloromethane (TTCM) at 90 ºC using alumina- and silica-supported platinum catalysts. The same research group obtained TOF values between 7.3 and 619 h^{-1} using Au, Pd and Au-Pd catalysts on Sibunit carbon.[50] In the case of HDC of dichloromethane (DCM), Bedia et al.[5] obtained TOF values in the range of 25.2-75.6 h^{-1} at 150 ºC using bimetallic Pt-Pd supported on sulfate zirconia catalysts. TOF values of around 0.9 h^{-1} at 120 ºC were reported for the HDC of DCM over alumina and sol–gel titania-supported Pd catalysts.[51]

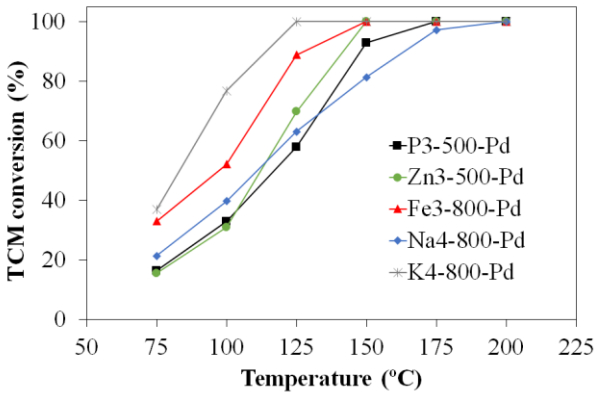

Fig. 6 TCM conversion versus reaction temperature (1000 ppmv inlet concentration and 0.8 kgcat·h·mol^{-1} TCM space time).

The purpose of the work is not only the removal of the chloromethane pollutant but also its valorisation upon transformation into more valuable hydrocarbons, preferably other than methane. In this sense, Figures 8A and B represent the evolution of selectivity with reaction temperature with (A) P3-500-Pd and (B) K4-800-Pd. The evolution of the selectivities of the rest of the catalysts follows similar trends (Figure ES5). The reaction products detected were, dichloromethane (DCM) and monochloromethane (MCM), as a result of the incomplete dechlorination of the TCM molecule, accompanied by methane, ethane and propane. Traces of butane were also detected. At low reaction temperatures methane is, for all the catalysts, the main reaction product, followed by ethane.

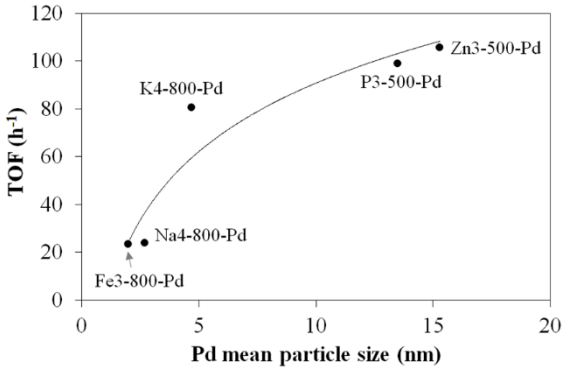

Fig. 7 TOF (100 ºC) versus Pd mean particle size.

Table 3 TOF values at different temperatures for the HDC of TCM.

Catalyst	Reaction temperature (ºC)	TOF (h^{-1})
P3-500-Pd	75	49.1
	100	98.8
	125	174.5
Zn3-500-Pd	75	52.9
	100	105.5
	125	238.0
Fe3-800-Pd	75	14.7
	100	23.2
	125	39.6
Na4-800-Pd	75	12.9
	100	23.9
	125	38.0
K4-800-Pd	75	38.6
	100	80.5
	125	104.9

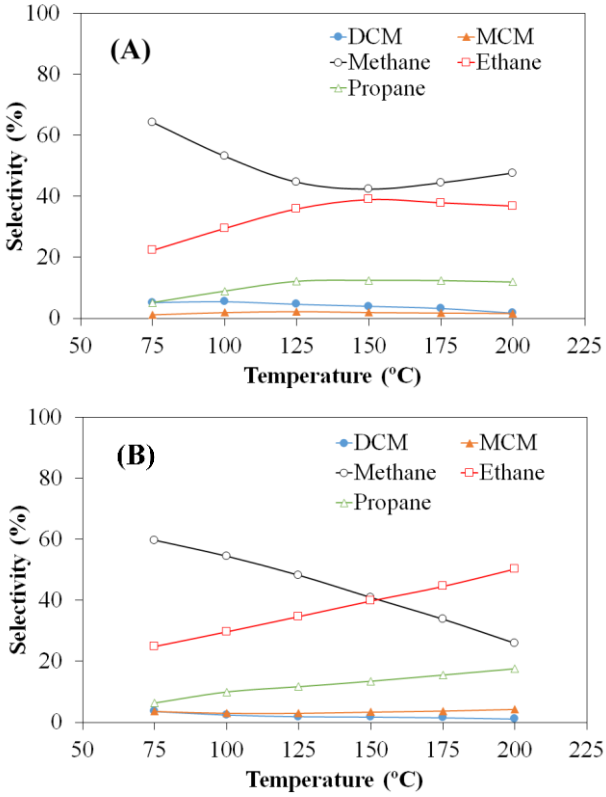

Fig. 8 Selectivity versus reaction temperature with (A) P3-500-Pd and (B) K4-800-Pd (τ = 0.8 kgcat·h·mol^{-1}; see conversion vs temperature in Figure 6).

With increasing temperature, the selectivity to methane decreases, increasing the selectivities to the target products ethane and propane and converting ethane in the main reaction product (except for P3-500-Pd, in which, methane is the main product in all the temperature range analysed). It is also noteworthy, the relatively low selectivities to the undesired incomplete dechlorination by-products, DCM and MCM, indicative of the high dechlorination degree achieved by the catalysts.

Figure 9 summarizes the selectivities to the different reaction products at 200 ºC, the temperature at which higher selectivities to ethane and propane were obtained. A catalyst based on a commercial activated carbon, Merck (A_{BET} = 783 m^2·g^{-1}) with 1.0 wt.% of Pd (deposited by the same procedure used for the rest of the catalysts) was included for comparison purposes. P3-500-Pd and Zn3-500-Pd show very similar behaviour to Merck-Pd, with selectivities to ethane and propane around 50%, and high dechlorination degrees (selectivities to DCM and MCM ≈ 5%). Fe3-800-Pd shows a slight increase in the selectivity to ethane and propane (≈ 60%). However, the most promising results were obtained with Na4-800-Pd and K4-800-Pd catalysts, which showed selectivities to the desired ethane and propane products of 77 and 68%, respectively (significantly higher than the approximately 50% obtained when using Merck-Pd). The outstanding results of Na4-800-Pd catalyst are negatively affected by the lower dechlorination degree obtained with this catalyst (selectivities to DCM and MCM ≈14%). However, K4-800-Pd catalyst besides excellent selectivity to the target compounds, exhibited also a high dechlorination degree. The

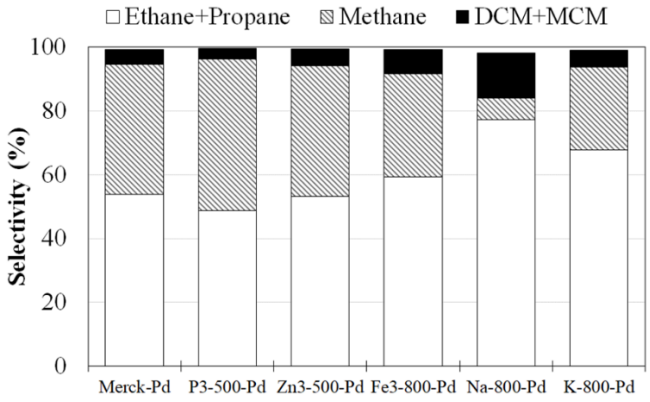

Fig. 9 Selectivities of the catalysts to ethane + propane, methane and DCM + MCM at 200 ºC (total TCM conversion).

higher selectivities to ethane and propane of Na4-800-Pd and K4-800-Pd could be associated to the lower Pd^0/Pd^{n+} ratios of these catalysts (Table 2). The higher proportion of electrodeficient Pd results in the higher selectivities to C2-C3 paraffins. This confirms that the formation of hydrocarbons with more carbon atoms than methane is enhanced by the combination of two chlorinated radicals adsorbed on adjacent electro-deficient metallic sites, suggested in previous studies.[52-55] The results here obtained show a higher influence of Pd oxidation state than of particle size on the selectivity. In contrast, particle size seems to have a greater influence on the activity of the catalysts. We have performed an additional test, with K4-800-Pd catalyst, analysing the HDC of TCM up to reaction temperatures of 400 ºC. At 300 ºC even better results were obtained with a selectivity to ethane and propane of more than 80% and a very high dechlorination degree (DCM was not detected and the selectivity to MCM was only 2.8%). A further increase of the reaction temperature up to 400 ºC leads to even a slight increase of the selectivity to ethane and propane (82.7%) and a further decrease of the selectivity to incomplete dechlorination products (no DCM, 1.6% MCM). However, at this temperature, the carbon balance fails by around 15%, due probably to the generation of condensation products at this high temperature with the consequent yield decrease and more probably future deactivation of the catalyst.

In this sense, we have analyzed the stability of the catalyst yielding the highest conversion, K4-800-Pd. Figures 10A and B represent the evolution of TCM conversion and selectivities upon time on stream at reaction temperatures of 100 and 200 ºC, respectively. At 100 ºC the conversion of TCM decreases continuously although at a moderate rate (after more than 50 h of reaction the conversion decreases from 76 to 62%). Furthermore, it seems that beyond 40 h on stream a pseudo-stationary state is reached, and TCM conversion decreases very slowly. Meanwhile, the selectivities to the different reaction products did not suffer significant modifications. At 200 ºC the catalyst showed an outstanding stability, yielding total conversion of TCM along the 60 h on stream of the experiment. Furthermore, the selectivities did not suffer significant changes and a very high dechlorination was maintained, with only traces of MCM detected and a selectivity to DCM below 5%. These results indicate a fairly good performance of the catalyst.

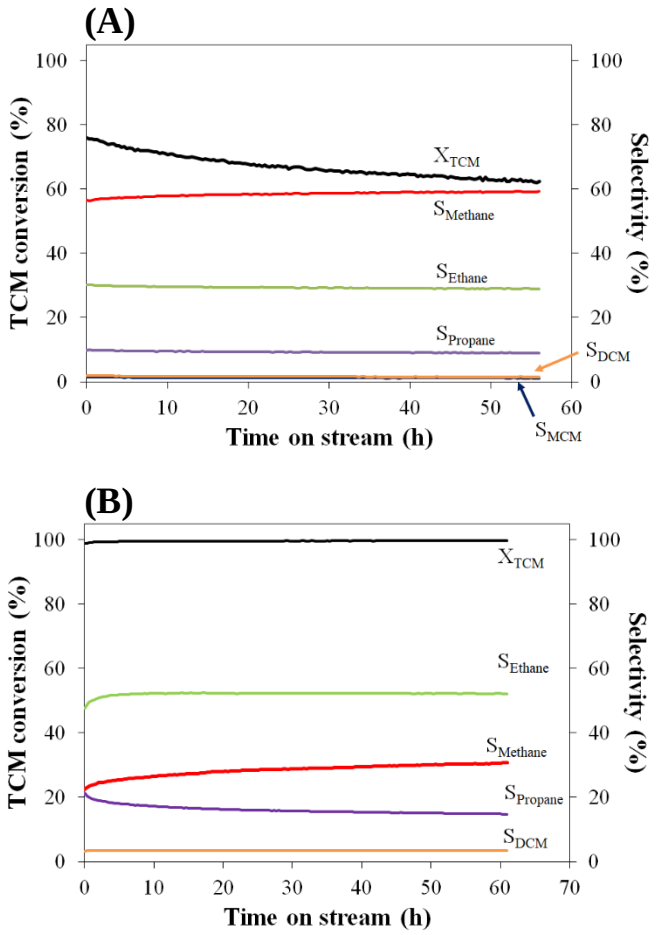

Fig. 10. Evolution of TCM conversion and selectivities upon time on stream with the K4-800-Pd catalyst at (A) 100 ºC, and (B) 200 ºC (1000 ppmv inlet concentration and 0.8 kgcat·h·mol-1 TCM space time).

Conclusions

Pd supported by incipient wetness impregnation on activated carbons obtained from lignin by chemical activation result in catalysts with good activity for the HDC of TCM. The use of different activating agents allows to obtain carbon-based catalysts with tuneable properties, such as, porosity, surface acidity, metallic to electrodeficient ratio or particle size of the active phase. TOF values in the range of around 12 to 240 h^{-1} were obtained in the temperature range analysed. In this work, the objective was to maximize the selectivity of the reaction to light paraffins, ethane and propane. The best results, in terms of dechlorination degree and selectivity to the target compounds, were obtained with the KOH derived catalyst, with a selectivity to ethane and propane of more than 80% and with a very high dechlorination degree at a reaction temperature of 300 ºC. This catalyst is characterized by a high surface area and low surface acidity which results in a low particle size (≈ 5 nm) and low Pd^0/Pd^{n+} ratio.

Conflicts of interest

There are no conflicts to declare.

Acknowledgements

The authors gratefully acknowledge financial support from the Spanish Ministerio de Economía y Competitividad (MINECO) through the project CTM 2014-53008. Also C. Fernández Ruiz acknowledges MINECO for his research grant.

References

1 E. Dobrzynska, M. Posniak, M. Szewczynska, B. Buszewski, *Crit. Rev. Anal. Chem.*, 2010, **40**, 41.
2 N. Ramírez, A. Cuadras, E. Rovira, F. Borrull, R.M. Marcé, *Environ. Int.*, 2012, **39**, 200.
3 B. Huang, C. Lei, C. Wei, G. Zeng, *Environ. Int.*, 2014, **71**, 118.
4 T. Mori, J. Kubo, Y. Morikawa, *Appl. Catal. A Gen.*, 2004, **271**, 69.
5 J. Bedia, A. Arevalo-Bastante, J.M. Grau, L.A. Dosso, J.J. Rodriguez, A. Mayoral, I. Diaz, L.M. Gómez-Sainero, *J. Catal.*, 2017, **352**, 562.
6 E. Diaz, A.F. Mohedano, J.A. Casas, C. Shalaby, S. Eser, J.J. Rodriguez, *Appl. Catal. B Environ.*, 2016, **186**, 151.
7 Z. Dong, X. Le, C. Dong, W. Zhang, X. Li, J. Ma, *Appl. Catal. B, Environ*, 2015, **162**, 372.
8 M. Ming, Y. Ren, M. Hu, Y. Zhang, T. Sun, Y. Ma, X. Li, W. Jiang, D. Gao, J. Bi, G. Fan, *Appl. Catal. B Environ.*, 2017, **210**, 462.
9 Z. Dong, X. Le, Y. Liu, C. Dong, J. Ma, *J. Mater. Chem. A*, 2014, **2**, 18775.
10 L.M. Kartashov, V.N. Rozanov, Y.A. Treger, M.R. Flid, T.L. Kalyuzhnaya, D.V. Tkach, *Catal. Ind.*, 2010, **2**, 230.
11 Y.A. Treger, V.N. Rozanov, E.A. Averina, *Catal. Ind.*, 2016, **8**, 107.
12 L.M. Gómez-Sainero, J. Palomar, S. Omar, C. Fernandez, J. Bedia, A. Álvarez-Montero, J.J. Rodriguez, *Catal. Today*, 2018, **310**, 75.
13 J. Bedia, L.M. Gómez-Sainero, J.M. Grau, M. Busto, M. Martin-Martinez, J.J. Rodriguez, *J. Catal.*, 2012, **294**, 207.
14 M. Martin-Martinez, L.M. Gómez-Sainero, J. Bedia, A. Arevalo-Bastante, J.J. Rodriguez, *Appl. Catal. B Environ.*, 2016, **184**, 55.
15 J. Chen, T. Guo, K. Li, L: Sun, *Catal. Sci. Technol., 2015, **5**, 2670.*
16 E. López, S. Ordonez, H. Sastre, F.V. Diez, *J. Hazard. Mater.*, 2003, **97**, 281.
17 T. Mori, T. Yasuoka, Y. Morikawa, *Catal. Today*, 2004, **88**, 111.
18 M. Martin-Martinez, L.M. Gómez-Sainero, M.A. Alvarez-Montero, J. Bedia, J.J. Rodriguez, *Appl. Catal. B Environ.*, 2013, **132–133**, 256.
19 M. Bonarowska, Z. Kaszkur, D. Lomot, M. Rawski, Z. Karpinski, *Appl. Catal. B Environ.*, 2015, **162**, 45.
20 J.M. Rosas, R. Ruiz-Rosas, J. Rodríguez-Mirasol, T. Cordero, *Chem. Eng. J.*, **2017**, 307, 707.
21 S.P.J.M. Carrot, M.M.L.R. Carrot, *Biores. Technol.*, 2007, **98**, 2301.
22 J. Bedia, J.M. Rosas, J. Rodríguez-Mirasol, T. Cordero, *Appl. Catal. B Environ.*, 2010, **94**, 8.
23 M. Martín-Martínez, M.F.F. Barreiro, A.M.T. Silva, J.L. Figueiredo, J.L. Faira, H.T. Gomes, *Appl. Catal. B Environ.*, 2017, **219**, 372.
24 E. Guillen, R. Rico, J.M. López-Romero, J. Bedia, J.M. Rosas, J. Rodríguez-Mirasol, T. Cordero, *Appl. Catal. A Gen.*, 2009, **368**, 113.
25 A. Lazzarini, A. Piovano, R. Pellegrini, G. Leofanti, G. Agostini, S. Rudić, M.R. Chierotti, R. Gobetto, A. Battiato, G. Spoto, A. Zecchina, C. Lambertiah, E. Groppo, *Catal. Sci. Technol.*, 2016, **6**, 4910.
26 A. Lazzarini, R. Pellegrini, A. Piovano, S. Rudić, C. Castan-Guerrero, P. Torelli, M.R. Chierotti, R. Gobetto, C. Lambertia, E. Groppo, *Catal. Sci. Technol.*, 2017, **7**, 4162.

27 S. Brunauer, P.H. Emmett, E. Teller, *J. Am. Chem. Soc*., 1938, **60**, 309.
28 B.C. Lippens, J.H. De Boer, *J. Catal*., 1965, **4**, 319.
29 M.M. Dubinin, V.A. Astakhov, *Bulletin of the Academy of Sciences of the URSS. Division of chemical science*, 1971, **20**, 3.
30 J. Freel, *J. Catal*., 1972, **25**, 139.
31 Y. Gao, Q. Yue, B. Gao, Y. Sun, W. Wang, Q. Li, Y. Wang, *Chem. Eng. J.,* 2013, **217**, 345.
32 V. Fierro, V. Torné-Fernández, A. Celzard, *Microp*. *Mesop. Mat.*, 2007, **101**, 419.
33 J.A. Zazo, J. Bedia, C.M. Fierro, G. Pliego, J.A. Casas, J.J. Rodriguez, *Catal. Today*, 2012, **187**, 115.
34 N.M.A. Al-Lagtah, A.H. Al-Muntaseb, M.N.M. Ahmad, Y. Salameh. *Microp. Mesop. Mat*., 2016, **225**, 504.
35 S.I. Mussatto, M. Fernandes, G.J.M. Rocha, J.J.M. Orfao, J.A. Texeira, I.C. Roberto. *Biores. Technol*., 2010, **101**, 2450.
36 E. González-Serrano, T. Cordero, J. Rodríguez-Mirasol, J.J. Rodriguez. *Ind. Eng. Chem. Res*., 1997, **36**, 4832.
37 G. Neri, M.G. Musolino, C. Milone, D. Pietropaolo, S. Galvagno. *Appl. Catal. A Gen*., 2001, **208**, 307.
38 W. Zhao, V. Fierro, C. Zlotea, M.T. Izquierdo, C. Chevalier-César, M. Latroche, A. Celzard, *Int. J. Hydrog. Energy*, 2012, **37**, 5072.
39 L.M. Gómez-Sainero, R.T. Baker, I.S. Metcalfe, M. Sahibzada, P. Concepción, J.M. López-Nieto, *Appl. Catal. A Gen*., 2005, **294**, 177.
40 L.M. Gómez-Sainero, R.T. Baker, A.J. Vizcaíno, S.M. Francis, J.A. Calles, I.S. Metcalfe, J.J. Rodríguez., *Ind. Eng. Chem. Res.*, 2009, **48**, 8364.
41 S. Wang, L. Wei, D. Yuanyuan, Y. Zhao, X. Ma, *Catal. Comm*., 2015, **72**, 43.
42 A.L.D. Ramos, P.D.S. Alves, D.A.G. Aranda, M. Schmal, *Appl. Catal. A Gen*., 2004, **277**, 71.
43 J. Bedia, R. Ruiz-Rosas, J. Rodríguez-Mirasol, T. Cordero, *J. Catal*., 2010, **271**, 33.
44 J. Bedia, R. Ruiz-Rosas, J. Rodríguez-Mirasol, T. Cordero, *AIChE J*., 2010, **56**, 1557.
45 J.F. Moulder, W.F. Stickle, P.E. Sobol, K.D. Bomben, J. Chastain, R.C. King Jr., Handbook of X-ray Photoelectron Spectroscopy, Physical Electronics Inc, Eden Prairie, MN, 1995.
46 L.M. Gómez-Sainero, J.M. Grau, A. Arcoya, X.L. Seoane, *Stud. Surf. Sci. Catal*., 2000, **130**, 2009.
47 V. Suresh Babu, M.S. Seehra, *Carbon* 1996, **34**, 1259.
48 M. Ouzzine, A.J. Romero-Anaya, M.A. Lillo-Ródenas, A. Linares-Solano, *Carbon*, 2014, **67**, 104.
49 M. Bonarowska, Z. Kaszkur, L. Kepinski, Z. Karpinski, *Appl. Catal. B Environ*., 2010, **99**, 248.
50 M. Bonarowska, Z. Kaszkur, D. Lomot, M. Rawski, Z. Karpinski, *Appl. Catal. B Environ*., 2015, **162**, 45.
51 C.A. Gonzalez, C.O.M. Patino, C. Montes de Correa, *Catal. Today,* 2008, **133–135**, 520.
52 A. Arevalo-Bastante, M.A. Álvarez-Montero, J. Bedia, L.M. Gómez-Sainero, J.J. Rodriguez, *Appl. Catal. B Environ*., 2015, **179**, 551.
53 M.A. Álvarez-Montero, L.M. Gómez-Sainero, J. Juan-Juan, A. Linares-Solano, J.J. Rodriguez, *Chem. Eng. J*., 2010, **162**, 599.
54 M.A. Álvarez-Montero, L.M. Gómez-Sainero, M. Martín-Martínez, F. Heras, J.J. Rodriguez, *Appl. Catal. B Environ*., 2010, **96**, 148.
55 M.A. Álvarez-Montero, L.M. Gómez-Sainero, A. Mayoral, I. Diaz, J.J. Rodriguez. *J. Catal*., 2011, **279**, 389.